Structural and Dynamic Characterization of the Aromatic Amino Acids of the Human Immunodeficiency Virus Type I Nucleocapsid Protein Zinc Fingers and Their Involvement in Heterologous $tRNA^{Phe}$ Binding: A Steady-State and Time-Resolved Fluorescence Study

Yves Mély,* Etienne Piémont,* Monica Sorinas-Jimeno,* Hugues de Rocquigny,‡ Nathalie Jullian,‡ Nelly Morellet,‡ Bernard P. Roques,‡ and Dominique Gérard*

*Laboratoire de Biophysique de la Faculté de Pharmacie, Université Louis Pasteur, Strasbourg I, 67401 Illkirch Cedex, and ‡Département de Chimie Organique, INSERM U266, Unité de Formation et de Recherches des Sciences Pharmaceutiques et Biologiques, 75270 Paris Cedex 06, France

ABSTRACT The steady-state and time-resolved fluorescence properties of two zinc-saturated 18-residue synthetic peptides with the amino acid sequence of the NH_2-terminal (NCp7 13–30 F16W, where the naturally occurring Phe was replaced by a Trp residue) and the COOH-terminal (NCp7 34–51) zinc finger domains of human immunodeficiency virus type I nucleocapsid protein were investigated. Fluorescence intensity decay of both Trp 16 and Trp 37 residues suggested the existence of two fully solvent-exposed ground-state classes governed by a $C = 2.2$ equilibrium constant. The lifetimes of Trp 16 classes differed from those of Trp 37 essentially because of differences in nonradiative rate constants. Arrhenius plots of the temperature-dependent nonradiative rate constants suggested that the fluorescence quenchers involved in both classes and in both peptides were different and the collisional rate of these quenchers with the indole ring was very low, probably because of the highly constrained peptide chain conformation. The nature of the ground-state classes was discussed in relation to ^1H nuclear magnetic resonance data. Using Trp fluorescence to monitor the interaction of both peptides with $tRNA^{Phe}$ we found that a stacking between the indole ring of both Trp residues and the bases of $tRNA^{Phe}$ occurred. This stacking constituted the main driving force of the interaction and modified the $tRNA^{Phe}$ conformation. Moreover, the binding of both fingers to $tRNA^{Phe}$ was noncooperative with similar site size (3 nucleotide residues/peptide), but the affinity of the NH_2-terminal finger domain ($K = 1.3 (\pm 0.2) 10^5 M^{-1}$) in low ionic strength buffer was one order of magnitude larger than the COOH-terminal one due to additional electrostatic interactions involving Lys 14 and/or Arg 29 residues.

INTRODUCTION

All retroviruses encode a *gag* gene product that is processed, subsequent to viral budding, by the retroviral protease to give several structural proteins, including the nucleocapsid protein. In human immunodeficiency virus type I (HIV-1), the nucleocapsid protein NCp15 is derived from the Pr55 gag polyprotein precursor and is ultimately processed into NCp7 and p6 in mature HIV virus (Di Marzo Veronese et al., 1987). Like most retroviral nucleocapsid proteins, HIV-1 NCp7 is highly basic and contains two motifs of the form $C\text{-}X_2\text{-}C\text{-}X_4\text{-}H\text{-}X_4\text{-}C$ (X = variable amino acid residue), which have been implicated in zinc binding (South et al., 1990; Fitzgerald and Coleman, 1991).

The three-dimensional structure of the two isolated zinc-saturated motifs has been determined from ^1H nuclear magnetic resonance (NMR) data (Summers et al., 1990; South et al., 1991). Both fingers have very similar folding patterns that include type I and type II NH-S tight turns and extensive internal hydrogen bonding. Both fingers also contain a single aromatic amino acid (Phe 16 in the NH_2-terminal and Trp 37 in the COOH-terminal finger motif), the side chain of which is directed away from the body of the peptide and toward the solvent. Recently the structure of the zinc-saturated NCp7 13–51 (Omichinski et al., 1991; Morellet et al., 1992) and NCp7 1–55 (Summers et al., 1992) was also determined, and it was revealed that the main structural features of the isolated finger motifs are conserved in these peptides.

In the capsid, the nucleocapsid protein is tightly associated to the dimeric RNA genome (Darlix et al., 1990) and is a key component of the viral life cycle. In vitro, the nucleocapsid protein has been shown to be involved in retroviral RNA dimerization, a process probably linked to specific genomic RNA packaging (Darlix et al., 1990) and annealing of the replication primer $tRNA^{Lys,3}$ to the initiation site of the reverse transcription (Barat et al., 1989, 1991). Point mutations that alter the first zinc finger of HIV-1 nucleocapsid protein result in a strong impairment of genomic RNA packaging (Aldovini and Young, 1990), indicating that the zinc finger motifs probably control the encapsidation of the viral genomic RNA. Nevertheless, replacement of both zinc fingers by a Gly-Gly linker did not inhibit the RNA binding and annealing activities of the nucleocapsid protein, whereas deletion of the short basic sequences ^{13}VK and $^{29}RAPRKKG^{35}$ flanking the first finger led to a complete loss of the NCp7 functions in vitro (De Rocquigny et al., 1992). Therefore it is suggested that the role of the zinc fingers might be to direct

Received for publication 30 July 1992 and in final form 23 June 1993.

Address reprint requests to Dr. Yves Mély, Faculté de Pharmacie, Laboratoire de Biophysique, 74, route du Rhin, B.P. 24, 67401, Illkirch Cedex, France.

Abbreviations used: HIV-1, human immunodeficiency virus type I; NMR, nuclear magnetic resonance; HEPES, *N*-(2-hydroxyethyl) piperazine-*N'*-2-ethane sulfonic acid; DAS, decay-associated spectra.

0006-3495/93/10/1513/10 $2.00

the spatial recognition by these short basic sequences of specific sites on the viral RNA and the replication primer tRNA. Within the zinc finger motif sequences, the aromatic residues (Phe 16 and Trp 37) are probably of critical importance since the replacement in related nucleocapsid proteins of one aromatic ring even with a hydrophobic moiety led to a large decrease in genomic RNA packaging (Méric and Goff, 1989; Dupraz et al., 1990). Thus the aromatic rings, through RNA intercalation, might cooperate with the basic domain to selectively recognize the packaging signal of the viral RNA in vivo (Morellet et al., 1992).

In this context, to gain further information about the structural and dynamic properties of the aromatic residues of the two finger motifs, we investigated their steady-state and time-resolved fluorescence properties in two zinc-saturated 18 residue synthetic peptides corresponding to the NH_2- and COOH-terminal zinc finger domain, respectively. In the NH_2-terminal finger motif, Phe 16 is only weakly fluorescent and was replaced by a Trp residue. Moreover, using the aromatic amino acid fluorescence properties, we investigated their involvement in the interaction of both fingers with the heterologous $tRNA^{Phe}$, which was taken as a model for the homologous $tRNA^{Lys,3}$.

MATERIALS AND METHODS

Solid-phase synthesis of NCp7 13–30 F16W and NCp7 34–51 (Fig. 1) was carried out using the stepwise solid phase method and 9-fluorenylmethoxycarbonyl (FMOC) amino acids on an automatic reprogrammed Applied Biosystems 431 A synthesizer as previously described (De Rocquigny et al., 1991). To preserve the highly oxidizable cysteine residues (purity > 99%), the lyophilized peptides were stored under vacuum. Prior to use, they were dissolved in freshly degassed buffer and poured immediately into anaerobic quartz cells, which maintain an inert argon atmosphere. The buffer was *N*-(2-hydroxyethyl)-piperazine-*N'*-2-ethane sulfonic acid) (HEPES) (5 mM, pH 7.5) for $tRNA^{Phe}$-binding experiments or HEPES (50 mM, KCl 100 mM, pH 7.5) for the other experiments. Each time, zinc was added to the peptide in a 1.5 molar ratio.

Absorption spectra were recorded on a Cary 4 spectrophotometer. Extinction coefficients of 5700 $M^{-1}\cdot cm^{-1}$ at 280 nm and 6.25×10^5 $M^{-1}\cdot cm^{-1}$, at 260 nm were used to determine the peptide and $tRNA^{Phe}$ concentrations, respectively. Difference spectra were recorded with tandem cells containing 800 μl of $tRNA^{Phe}$ and peptide into the separate compartments. After the baseline was recorded, the solutions of the sample cell were mixed thoroughly and the difference spectrum was recorded. The baseline was checked once again after the solutions were mixed in the reference cell.

Fluorescence spectra were performed at 20 ± 0.5°C with a SLM 48000 spectrofluorometer. Quantum yields were determined taking L-Trp in water (Φ = 0.14) as a reference (Eisinger and Navon, 1969).

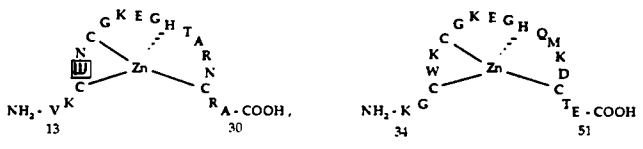

FIGURE 1 Amino acid sequences of NCp7 13–30 F16W and NCp7 34–51. In the first finger the naturally occurring Phe 16 was replaced by a Trp residue.

Fluorescence lifetime measurements were performed using the time-correlated single photon counting technique. A complete description of the device has been reported elsewhere (Lami and Piémont, 1992). The output of a Spectra-Physics mode-locked argon laser was used to synchronously pump a rhodamine 6G dye laser that was cavity dumped at 0.8 MHz and then frequency doubled. Fluorescence excitation was at 295 nm, with emission collected from 310 to 410 nm through a 4-nm bandpass monochromator (Jobin-Yvon H10) combined with a cutoff filter to reduce the residual diffusion of the excitation light. The data were recorded on a multichannel analyzer (Ortec 7100) calibrated at 106 ps/channel. The instrumental response function was approximated by the observed decay of a strongly quenched fluorophore of negligible lifetime (<20 ps) (*p*-terphenyl in cyclohexane + CCl_4 mixture, 2:1 v/v) (Kolber and Barkley, 1986). The decay data were analyzed as a sum of exponentials:

$$I(t) = I_0 \sum \alpha_i e^{-t/\tau_i} \quad (1)$$

where $I(t)$ and I_0 are the intensities at time t and $t = 0$ respectively, α_i's are the normalized preexponential terms such as $\sum \alpha_i = 1$, and τ_i's are the lifetime components. Time-resolved fluorescence data were analyzed via this multiexponential form by an iterative reconvolution procedure based on the estimated covariance matrix (Lami and Piémont, 1992). Since up to 20 decays were accumulated for each sample, confidence intervals of the mean recovered decay parameters were estimated using Hotelling's T^2 statistics. The number of exponentials was progressively increased until the fit did not improve. The adequacy of the fit was judged by reduced χ^2, weighted residuals, and the autocorrelation of the weighted residuals.

The fractional intensities f_i of each species were calculated using $f_i = \alpha_i\tau_i / \sum \alpha_i\tau_i$, and the mean fluorescence lifetime $\langle\tau\rangle$ was calculated using $\langle\tau\rangle = \sum \alpha_i\tau_i$. Decay-associated spectra (DAS) were calculated from the steady-state fluorescence intensity $F_{ss}(\lambda)$ and the time-resolved parameters using

$$F_i(\lambda) = F_{ss}(\lambda)\alpha_i(\lambda)\tau_i(\lambda) \Big/ \sum \alpha_i(\lambda)\tau_i(\lambda) \quad (2)$$

Temperature-dependent lifetime measurements were performed in thermostated quartz cells.

Fluorescence quenching by acrylamide was carried out by adding aliquots from an acrylamide stock solution to the peptides. As acrylamide did not alter the overall shape of the fluorescence spectrum, changes in the fluorescence intensity at 351 nm were recorded. Data were corrected for the dilution and for the screening effects due to the absorption of acrylamide at 295 nm (Hélène et al., 1971).

The binding of $tRNA^{Phe}$ to the zinc finger peptides was monitored by adding small aliquots of $tRNA^{Phe}$ to a peptide solution and following the fluorescence decrease of the Trp residues with a SLM 48000 (at 20°C) spectrofluorometer. The excitation wavelength was 280 or 295 nm, and the emission wavelength was 350 nm. Fluorescence intensities were corrected for dilution, buffer fluorescence, and screening effects by added $tRNA^{Phe}$ (Hélène et al., 1971). Control experiments in the absence of protein showed that the Y base fluorescence is negligible in these conditions and needs no further correction. Binding isotherms were analyzed using the equation of McGhee and von Hippel (1974) for noncooperative binding:

$$\nu/L = K(1 - n\nu)[(1 - n\nu)/(1 - (n - 1)\nu)]^{n-1}, \quad (3)$$

where ν is the binding density of the ligand (peptide) on the lattice (nucleic acid), L is the free ligand concentration, n is the binding site size, and K is the intrinsic binding constant. The binding density ν is given by $\nu = [(I_0 - I)/(I_0 - I_{min})](Pt/Nt)$, where Pt is the peptide concentration, Nt is the total lattice residue concentration, and I_0, I, and I_{min} are the peptide fluorescence in the absence and in the presence of a given and a saturating nucleotide concentration, respectively. The nonlinear least-squares fit of Eq. 3 to experimental data was performed using the algorithm of Kowalczykowski et al. (1986). Binding isotherms showed no evidence for any cooperativity, and the use of the McGhee and von Hippel (1974) equation for cooperative binding yielded poorer fits than the noncooperative one.

Salt reversal of the binding of the peptide to $tRNA^{Phe}$ was monitored by following the peptide fluorescence increase brought about by the addition

of a 3 M NaCl solution. Calculation of the affinity K was performed using Eq. 3 with the assumption that n was constant throughout the range of [NaCl] used.

RESULTS

Fluorescence properties of Trp residues in NCp7 13–30 F16W and NCp7 34–51

Absorption spectra of NCp7 13–30 F16W and NCp7 34–51 were very similar to the spectra of *N*-acetyl-L-tryptophanamide in water, exhibiting a maximum at 280 nm and two pronounced shoulders at 273 and 288 nm, respectively (data not shown). The emission spectra of the two peptides also were similar, with a maximum emission wavelength at 353 (±1) nm, but their quantum yields were different: 0.175 (±0.004) and 0.207(±0.004) for NCp7 13–30 F16W and NCp7 34–51, respectively.

To investigate further the spectral differences between the two peptides, their fluorescence decays were analyzed according to the emission wavelength by time-correlated single photon counting. In both cases at wavelengths equal or greater than 340 nm, the fluorescence decay was adequately fitted ($\chi^2 = 1.1$) by a biexponential decay with a major long-lived fluorescence lifetime contributing to 90% of the total intensity and a minor shorter one (Table 1). The addition of a third component did not improve the accuracy of the fit. In contrast, on the blue end of the spectrum, a short, subnanosecond component (<200 ps) representing less than 2% of the fluorescence intensity significantly improved the fit. As already reported for other proteins (Green et al., 1990; Chabbert et al., 1992), this component was probably due to Rayleigh and Raman scattering and did not significantly affect the observed time-resolved spectra. Consequently, at these wavelengths only the two main components were taken into account, with their preexponential terms normalized to have a sum equal to 1. Fig. 2 summarizes the parameters describing the fluorescence decay throughout the spectrum. The two lifetimes τ_1 and τ_2 of both peptides were roughly independent of the wavelength (Fig. 2 *a*). Clearly, both τ_1 and τ_2 values of NCp7 13–30 F16W were shorter than the corresponding values of NCp7 34–51, whereas the normalized preexponential terms were similar and vary identically with the wavelength (Fig. 2 *b*). On the assumption that the biexponential decay kinetics arise from ground-state heterogeneity (see Discussion), the steady-state spectrum could be resolved

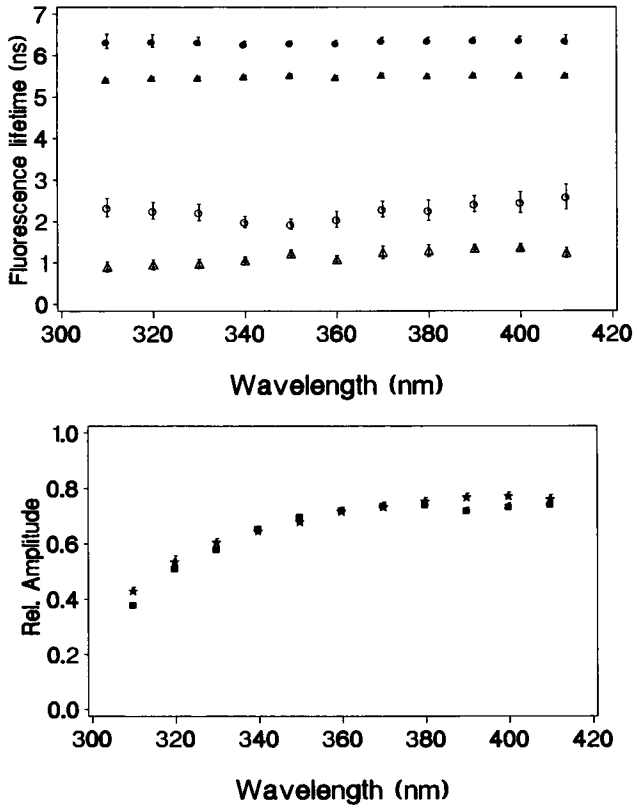

FIGURE 2 Wavelength dependence of the fluorescence decay parameters of HIV-1 NCp7 zinc fingers. The long-lived (●, ▲) and short-lived (○, △) lifetimes (*a*) of NCp7 13–30 F16W (▲, △) and NCp7 34–51 (●, ○) and the long-lived component relative amplitude (*b*) of NCp7 13–30 F16W (■) and NCp7 34–51 (★) are plotted versus the fluorescence emission wavelength. The excitation wavelength is 295 nm. At wavelengths ≤ 330 nm, the data plotted corresponded to the two main components of the decay fitted with three exponentials (see text). The confidence intervals at the 5% level of significance were determined as described in Materials and Methods. In (*b*) confidence intervals were within experimental points.

TABLE 1 Fluorescence decay parameters of NCp7 13–30 F16W and NCp7 34–51

	τ_i (ns)	α_i (%)	f_i (%)	$k_f \times 10^{-7}$ (s^{-1})	$k_{nri} \times 10^{-8}$ (s^{-1})	$\langle\tau\rangle$ (ns)
NCp7 13–30 F16W*	1.1 (±0.1)	31.5 (±0.7)	8 (±1)	4.3 (±0.2)	8.7 (±0.5)	4.1 (±0.1)
	5.52 (±0.02)	68.5 (±0.8)	92 (±1)	4.3 (±0.2)	1.38 (±0.03)	
NCp7 34–51‡	1.9 (±0.1)	32 (±1)	12 (±1)	4.2 (±0.2)	4.8 (±0.3)	4.9 (±0.1)
	6.32 (±0.04)	68 (±1)	88 (±1)	4.2 (±0.2)	1.16 (±0.03)	

The peptide concentrations were about 20 μM. Excitation and emission wavelengths were 295 and 350 nm, respectively. Lifetime components τ_i, normalized preexponential terms α_i, fractional intensities f_i, and mean lifetime $\langle\tau\rangle$ were expressed as means (± confidence intervals at the 5% level of significance). The radiative rate constant k_f and the nonradiative rate constant k_{nri} were calculated using $k_f = \Phi/\langle\tau\rangle$ and $k_{nri} = 1/\tau_i - k_f$, respectively.

* Identical decay parameters were obtained in the presence of 12, 30, and 60 μM $tRNA^{Phe}$ (nucleotide concentration), which decreased the steady-state fluorescence by 20, 38, and 59%, respectively.

‡ Identical decay parameters were obtained in the presence of 45, 120, 195, and 345 μM $tRNA^{Phe}$, which decreased the steady-state fluorescence by 36, 45, 54, and 66%, respectively.

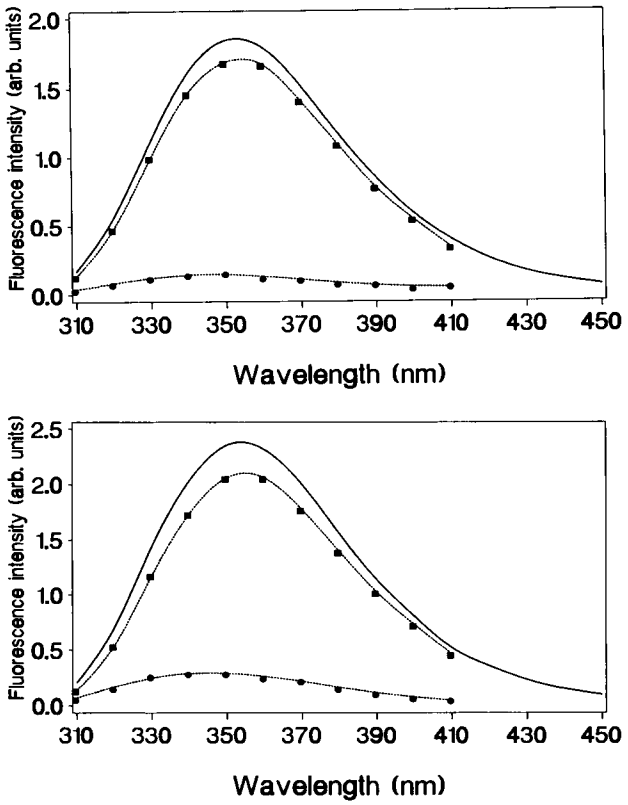

FIGURE 3 Resolution of NCp7 13–30 F16W (*a*) and NCp7 34–51 (*b*) fluorescence emission spectrum into two spectra associated with the long-lifetime component (■) and the short-lifetime component (●). The solid line represents the steady-state fluorescence spectrum under the same experimental conditions.

into two components (DAS) associated with each particular lifetime (Fig. 3 *a* and *b*). The fluorescence emission of both peptides was dominated by the long-lived component spectrum, the maximum emission (355 nm) of which was similar to that of the steady-state spectrum. The spectrum of the short-lived component was 5 to 10 nm blue-shifted as compared to that of the long-lived component and only contributed about 10% of the total fluorescence intensity.

To get further insight in the fluorescence desexcitation pathway, the fluorescence decays of both peptides were studied at 350 nm emission wavelength over the 10–60°C range. The fluorescence decays could be described at all temperatures as a sum of two exponentials ($\chi^2 < 1.2$). The long-lived component decreased sharply from 6.63 ns at 9.2°C to 3.30 ns at 59°C for NCp7 13–30 F16W and from 7.3 ns at 9.8°C to 2.6 ns at 58.8°C for NCp7 34–51. In contrast, the short-lived component was less sensitive to temperature, especially in the case of NCp7 13–30 F16W. In both peptides, the normalized preexponential term of the long-lived component was almost constant in the 10–50°C range and decreased only at higher temperatures. According to previous work on indole derivatives, the nonradiative pathway of tryptophan may be divided into temperature-dependent and -independent mechanisms (Robbins et al., 1980; Chang et al., 1983; Petrich et al., 1983). The temperature-dependent nonradiative decay rate k_{nrti} of the *i*th lifetime component is given by $k_{nrti} = (1/\tau_i) - k_f - k_{isc}$, where the temperature-independent parameters k_f and k_{isc} are the radiative rate constant and the intersystem crossing rate, respectively. In keeping with the red-shifted DAS, the radiative decay rates, k_f of the two emitting species were assumed to be similar and thus equal to the $\Phi/\langle\tau\rangle$ ratio (Chen et al., 1991). The calculated k_f values (Table 1) were identical for the two peptides and close to those obtained for *N*-acetyl-L-tryptophanamide and different indole derivatives in water (Ricci et al., 1970; Werner and Forster, 1979), suggesting that the quenching mechanisms are essentially dynamic in nature. The intersystem crossing rate k_{isc} was assumed to be 3.3×10^7 s^{-1} (Petrich et al., 1983). The Arrhenius plots (Fig. 4) were obtained, following the method of Robbins et al. (1980), by plotting $\ln(k_{nrti})$ versus $1/T$ (K). In both fingers, Arrhenius plots of the long-lived component gave a straight line with an activation energy of 19.9 (±0.1) and 25.1 (±0.8) kJ·mol^{-1} for NCp7 13–30 F16W and NCp7 34–51, respectively. The corresponding frequency factors were $3.8\ (\pm0.1) \times 10^{11}$ and $2.6\ (\pm0.5) \times 10^{12}$ s^{-1}, respectively. For the short-lived component, the results are less straightforward. A straight line was obtained for NCp7 34–51 with an activation energy of 16 (±2) kJ·mol^{-1} and a frequency factor of $4(\pm2) \times 10^{11}$ s^{-1}, but not for NCp7 13–30 F16W, for which a plateau was reached above 35°C.

Finally, to obtain further information about the two components of both Trp residues, fluorescence quenching by acrylamide was carried out. The quenching curves of both peptides clearly showed an upward curvature (Fig. 5) and were treated by using $F/F_0 = \Sigma f_i/(1 + K_i[Q])e^{V_i[Q]}$ (4), where F_0 and F are the fluorescence intensities at 350 nm in the absence and in the presence of quencher Q, f_i is the fraction of the fluorescence due to component i, and K_i and V_i are the respective collisional and static quenching constants (Eftink and Ghiron, 1976). The collisional constant K_i is given by $kq_i \cdot \tau_i$, where kq_i is the quenching rate constant and τ_i is the fluorescence lifetime of component i in the absence of

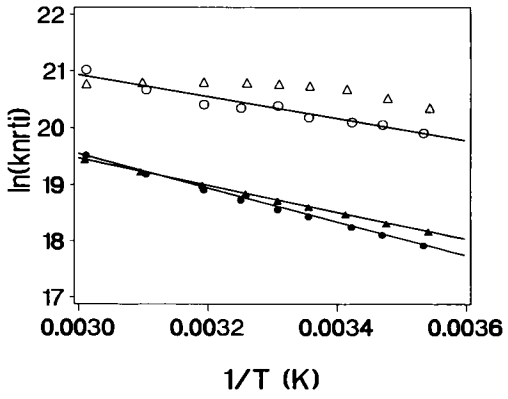

FIGURE 4 Arrhenius plots obtained from the short-lifetime (○, △) and the long-lifetime (●, ▲) components of NCp7 13–30 F16W (△, ▲) and NCp7 34–51 (○, ●). The calculation of the temperature-dependent nonradiative rate constant k_{nrti} is given in the text.

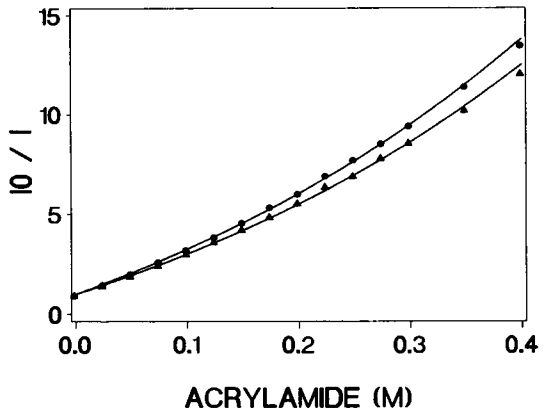

FIGURE 5 Stern-Volmer plots of NCp7 13–30 F16W (▲) and NCp7 34–51 (●) quenching by acrylamide. Solid lines represent the theoretical quenching calculated using Eq. 4.

quencher. By making the reasonable assumption that the static quenching constant V_i was identical for the two classes, the data could be adequately fitted using identical kq_i values for the different species (Fig. 5). Allowing the kq_i to vary did not significantly improve the fit and gave very similar results (data not shown). The bimolecular quenching constants (kq_i = 3.4 (±0.1) × 10^9 $M^{-1}\cdot s^{-1}$) and static quenching constants (V_i = 1.3 (±0.1) M^{-1}) of both peptides were high and identical, suggesting that the two components of both Trp residues corresponded to fully solvent-exposed species.

Interaction of NCp7 13–30 F16W and NCp7 34–51 with $tRNA^{Phe}$

The addition of $tRNA^{Phe}$ to both peptides induced a very large fluorescence decrease in their Trp residues. Irrespective of the initial peptide concentration, the residual fluorescence of NCp7 13–30 F16W and NCp7 34–51 at the highest concentrations of $tRNA^{Phe}$ added was less than 5 and 10%, respectively, suggesting that both Trp 16 and Trp 37 are almost completely quenched in the peptide-$tRNA^{Phe}$ complex. Such a behavior has already been described for several model peptides (Brun et al., 1975; Montenay-Garestier et al., 1983; Rajeswari et al., 1987) and has been assigned to a stacking of the indole moiety of the Trp residue with nucleic acid bases. To confirm this hypothesis, the fluorescence decay of both peptides was monitored in the presence of various $tRNA^{Phe}$ concentrations. Clearly, neither the fluorescence lifetime nor the preexponential terms were markedly modified by the presence of $tRNA^{Phe}$ (Table 1). Only the highest concentration of $tRNA^{Phe}$ added to NCp7 13–30 F16W, which decreased the steady-state fluorescence to about 90%, induced the appearence of a third short component (data not shown). This is probably without significance since in this condition, the fluorescence of the buffer and the nucleotides is no more negligible. Thus, Trp 16 and Trp 37 are completely quenched (within experimental limitations of our lifetime measurements) in $tRNA^{Phe}$-peptide complexes, in keeping with stacking with the bases of $tRNA^{Phe}$. Since $tRNA^{Phe}$ contained the unusual Y base, the absorption spectrum of which overlaps the Trp emission spectrum, it was necessary to check whether energy transfer did not contribute to the Trp fluorescence decrease. For this purpose the emission spectra that were performed, in the presence of various $tRNA^{Phe}$ concentrations, at 295 nm (where both Trp and Y base absorb) excitation wavelength were compared in the 480–600 nm range (where only the Y base fluoresces) with those performed at 310 nm (where only the base absorbs) excitation wavelength. This comparison is very convenient since in the absence of protein, the emission spectra of $tRNA^{Phe}$ at these two excitation wavelengths were superimposable. In the presence of protein no significant difference could be observed whatever the $tRNA^{Phe}$ concentration used, suggesting that energy transfer between Trp and Y base was negligible (data not shown). To further characterize the $tRNA^{Phe}$-peptide complex, the difference absorption spectra obtained after mixing the peptides with $tRNA^{Phe}$ were recorded (Fig. 6). The difference spectra of both peptides were rather similar, with a strong negative peak around 245 nm, a small negative peak at 288 nm, and a positive peak at 295–300 nm. This positive peak is characteristic of the stacking of Trp with bases (Toulmé and Hélène, 1980) and thus confirmed our previous hypothesis.

Using the $tRNA^{Phe}$-induced fluorescence decrease, we determined the binding parameters of the peptide-$tRNA^{Phe}$ interaction (Fig. 7). For both peptides the affinities were low, and this indicated to us the necessity of working in low ionic strength buffer. The binding site size was found to be identical in the two peptides (n = 3), but the affinity of NCp7 13–30 F16W was about 15 times greater than that of NCp7 34–51 (Table 2). The binding site size of NCp7 13–30 F16W could be determined independently using the intersection of the tangential to the low [$tRNA^{Phe}$]/[peptide] ratios (where the binding is assumed to be stoichiometric) with the x-axis in a fluorescence intensity versus [$tRNA^{Phe}$]/[peptide] plot. This intersection is about 3 (Table 2), in good agreement with the calculated value. The affinity of NCp7 34–51 was too low

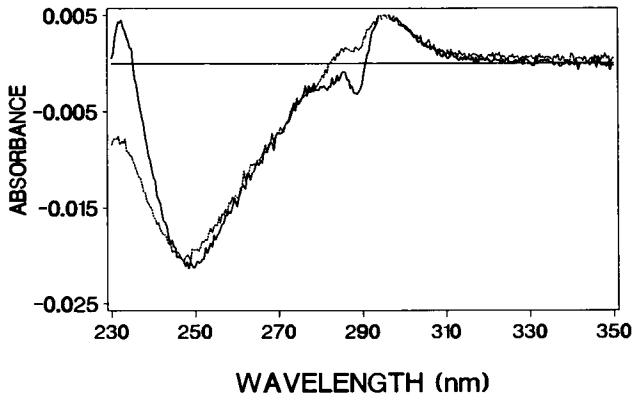

FIGURE 6 Difference absorption spectra of $tRNA^{Phe}$ in the presence of NCp7 13–30 F16W (——) and NCp7 34–51 (- - - -). The concentrations of $tRNA^{Phe}$ (nucleotides) and NCp7 13–30 F16W were 102 μM and 12 μM, respectively, while those of the NCp7 34–51 complex were 117 μM and 17 μM, respectively.

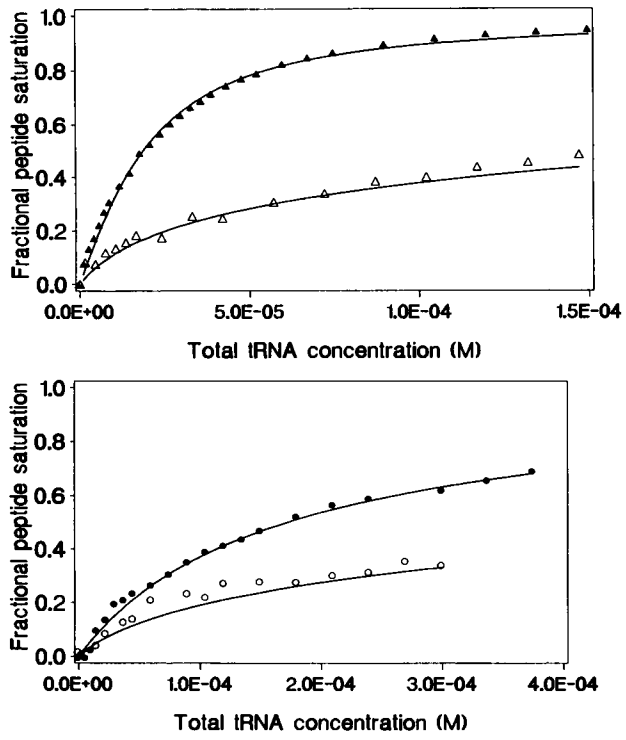

FIGURE 7 $tRNA^{Phe}$-binding isotherms of NCp7 13–30 F16W (*a*) and NCp7 34–51 (*b*). The experiments were performed in 5 mM HEPES either in the absence (●, ▲) or in the presence (○, △) of 1 mM Mg^{2+}. The concentrations of NCp7 13–30 F16W (▲, △) and NCp7 34–51 (●, ○) were 4.6 μM and 7.8 μM, respectively, in the absence of Mg^{2+} and 9.7 μM and 12 μM, respectively, in the presence of 1 mM Mg^{2+}. Solid lines represent the best fit for values of K and n given in Table 2.

to allow this independent estimation of n. In the presence of 1 mM Mg^{2+}, the binding affinities were decreased by a factor of 14 and 3 for NCp7 13–30 F16W and NCp7 14–51, respectively. The fits in the presence of Mg^{2+} were fair and were not improved by using cooperative models (McGhee and von Hippel, 1974). The addition of concentrated NaCl to NCp7 13–30 F16W-$tRNA^{Phe}$ complexes brought about a partial reversal of the peptide fluorescence decrease, suggesting that the complex formation depends on ionic interactions (Fig. 8 *a*). In contrast, the reversal for NCp7 34–51 was almost nil, indicating that ionic interactions were negligible. The plots of log K versus log [NaCl] were linear for both peptides but differed by their slopes (Fig. 8 *b*). The slopes were analyzed according to the method of Record et al. (1976): $(-\delta \log K)/(\delta \log[\mathrm{NaCl}]) = k + m'\psi$, where k is the number of anions displaced by the interaction, m' is the number of ion pairs formed between protein and nucleic acid, and ψ is the fraction of counterion bound per lattice charge. ψ was estimated to be close to the 0.71 value of a single-stranded DNA. Moreover, as k is also undetermined, only an upper limit for the number of ion pairs m' can be calculated (Table 2). In both peptides m' was lower than 1.0, suggesting that ionic interactions were rather weak. These ionic interactions were even further decreased in the presence of 1 mM Mg^{2+}. In contrast to the slopes, the extrapolated values of log K at 1 M NaCl, which are related to the nonelectrostatic interactions, were similar for the two peptides in the presence and in the absence of Mg^{2+} (Table 2).

DISCUSSION

NCp7 13–30 F16W and NCp7 34–51 conformational and dynamic properties

Fluorescence spectroscopy of zinc-saturated NCp7 13–30 F16W and NCp7 34–51 has provided a detailed description of the structural and dynamic properties of the individual aromatic residues of NCp7 zinc fingers. The two peptides have largely similar amino acid compositions (Fig. 1) and three-dimensional structures (Summers et al., 1990; South et al., 1991), suggesting that Trp residues are in similar environments and thus have similar desexcitation pathways. The fluorescence intensity decays of both Trp 16 and Trp 37 are biexponential, suggesting either ground-state or excited-state heterogeneity. The invariance of the lifetime values with wavelength and the time-resolved spectra of both peptides suggest that excited-state solvation on the nanosecond time scale does not occur and that the emission of Trp is clearly from a fully solvent-relaxed excited state. Other excited-state reactions can also be ruled out since no negative preexponential factor could be detected at any emission wavelength and since the Trp residues of the two peptides have similar preexponential terms but different lifetimes. The latter assertion indeed could not be reconciled with excited-state models, since in these models both preexponential terms and lifetimes are complex linked functions (Lakowicz, 1983; Alcala et al., 1987), and thus a change in fluorescence lifetime would necessarily modify the preexponential terms. The biexponential decay kinetics from both Trp's are entirely consistent with the existence of a ground-state equilibrium as previously proposed for Trp (Szabo and Rayner, 1980) and several single solvent-exposed Trp residues in peptides (Cockle and Szabo, 1981; Ross et al., 1981, 1992; Mély et al., 1993). In fact, it is probably more correct to relate the decay times and DAS to classes of conformations rather than to unique precise conformations since subnanosecond protein motions have been largely reported (Brooks et al., 1988; Frauenfelder et al., 1988, and references therein), and thus the interconversion rates between the conformations accessible within a class could be much faster than the fluorescence decay time.

Since the two highly solvent-exposed ground-state classes in both peptides probably have similar radiative rate constants and extinction coefficients, the equilibrium constant C between the two classes can be readily obtained from the integrated fluorescence intensities: $C = c_2/c_1 = S_2 \cdot \tau_1/S_1 \cdot \tau_2$ (where c_i and S_i are the concentration and the area under the DAS of component i, respectively). C is about 2.2 at 20°C for both peptides and is probably thermodynamically imposed by the highly constrained peptide chain conformation. Moreover, as C is almost invariant in the 10–50°C range,

TABLE 2 tRNA^{Phe}-binding parameters of NCp7 13–30 F16W and NCp7 34–51

	$[Mg^{2+}]$ (mM)	K (M^{-1})	n	$\delta \log K/\delta \log$ [NaCl]	m'	$\log K$ (1 M)
NCp7 13–30 F16W	0	1.3 (±0.2)×10^5*	3.0 (±0.5) 3.2 (±0.3)‡	−0.60 (±0.05)	0.85 (±0.07)	3.53 (±0.03)
	1	9 (±2) ×10^3	2.8 (±0.6)	−0.34 (±0.06)	0.48 (±0.08)	3.2 (±0.2)
NCp7 34–51	0	8.4 (±0.7)×10^3	2.9 (±0.7)	−0.16 (±0.03)	0.23 (±0.04)	3.5 (±0.1)
	1	2.6 (±0.5)×10^3	2.7 (±0.6)	−0.12 (±0.06)	0.17 (±0.08)	3.4 (±0.1)

* Each parameter was expressed as the mean ± SEM of at least five independent experiments.
‡ Determined independently with the tangential to the low [tRNA^{Phe}]/[peptide] concentrations, as indicated in the text.

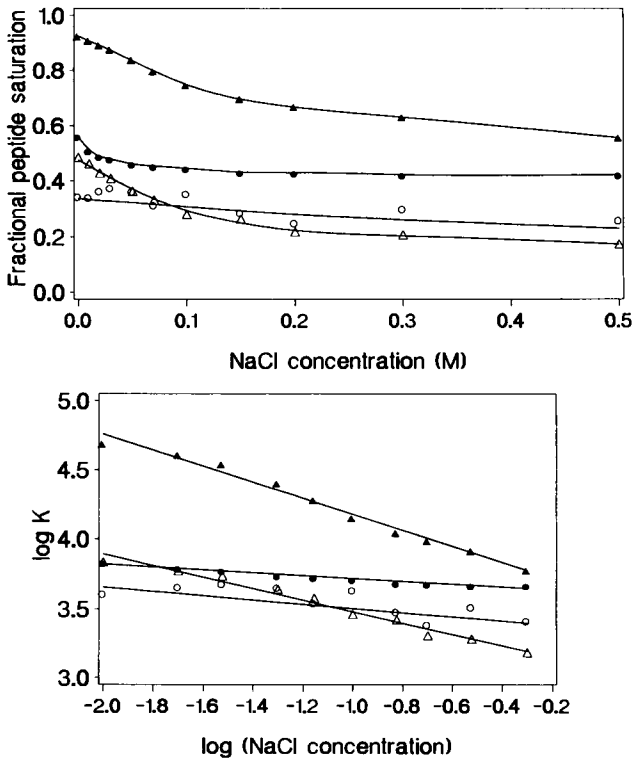

FIGURE 8 Reversal of tRNA^{Phe}-NCp7 13–30 F16W and -NCp7 34–51 interaction by NaCl. Symbols are as in Fig. 7. The tRNA^{Phe} and NCp7 13–30 F16W concentrations were, respectively, 150 μM and 4.5 μM in the absence of Mg^{2+} and 147 μM and 9.7 μM in the presence of Mg^{2+}. The tRNA^{Phe} and NCp7 34–51 concentrations were, respectively, 173 μM and 7.9 μM in the absence of Mg^{2+} and 300 μM and 12 μM in the presence of Mg^{2+}. (*a*) Fractional peptide saturation versus [NaCl] plot; (*b*) log K versus log([NaCl]) plot according to Record et al. (1976).

the entropy and enthalpy changes associated with the equilibrium are low ($|\Delta H°| < 3$ kJ·mol^{-1} and $|\Delta S°| < 5$ J·K^{-1}mol^{-1}).

In both peptides, the two classes differ essentially in their nonradiative rate constants. As ^{1}H NMR data clearly indicate that the closest quenchers to Phe 16 and Trp 37 in both fingers are essentially peptide carbonyl groups (Morellet et al., 1992), we may reasonably conclude that the main nonradiative pathway is a charge transfer between Trp (which is the donor) and the carbonyl groups (the acceptors). According to the model for charge transfer developed by Hopfield (1974, 1977), the activation energy calculated from the Arrhenius plots of the temperature-dependent nonradiative rate constants depends on the ionization potential of the donor and the electron affinity of the acceptor, while the frequency factor depends on the distance and orientation of the donor with respect to the acceptor. The ground-state classes of NCp7 34–51 essentially differed in their activation energies, suggesting that at least a part of the involved quenchers is different. We speculate that the more efficient quenchers of the short-lifetime class may correspond to carbonyl groups with increased electron affinity because of an interaction of these groups with one or more of the numerous positively charged residues present in the zinc finger motif. A similar conclusion is obtained when the long-lifetime classes of both peptides are compared, the most efficient quenchers being those of NCp7 13–30 F16W. The low frequency factors obtained for each class are in keeping with the highly constrained peptide chain conformation, which probably limits the collision rate of the indole moiety with the neighboring quenchers. As the Arrhenius plot of the short-lifetime class of NCp7 13–30 F16W was not linear, it is suggested that either a somewhat more complicated deactivation pathway may occur in this case or that structural constraints may limit the increase in the nonradiative rate constant to a value that cannot be overcome without disrupting the folded backbone conformation.

As the exact nature of the conformers could not be deduced from fluorescence data alone, the latter are discussed in relation to ^{1}H NMR data and molecular modeling of NCp7 13–51 (Morellet et al., 1992). The peptide chain backbones of the two fingers were shown to be largely superimposable, excluding them as a possible source of ground-state heterogeneity. As rotation of the indole ring about the C^α-C^β and/or C^β-C^γ bonds of Trp residues in proteins is thought to be a restricted process (Szabo and Rayner, 1980), it is tempting to attribute the exponentials to ground-state χ^1 or χ^2 rotamers about the C^α-C^β and C^β-C^γ bonds, respectively. The existence of such rotamers has been clearly demonstrated in [Trp^2] oxytoxin (Ross et al., 1992) and variant-3 scorpion neurotoxin (Haydock et al., 1990) and suggested in many other proteins (Cockle and Szabo, 1981; Ross et al., 1981; Mély et al., 1993). The standard free energy $\Delta G° = -RT\ln C$ of the equilibrium between the two fluorescent classes is about −2 kJ·mol^{-1} and is comparable to that obtained for Trp

47 rotamers in variant-3 scorpion neurotoxin (Haydock et al., 1990). Moreover, the inferred very low enthalpy and entropy changes are also in keeping with the very localized conformational changes implied in the rotamer model. Furthermore, since no excited-state reaction could be observed by time-resolved fluorescence and since the indole moiety protons gave sharp resonances by ^{1}H NMR (Morellet et al., 1992), we may further conclude that the interconversion rates between the two classes are between 10^3 and 5×10^7 s^{-1}, in keeping with those in [Trp^2] oxytoxin (Ross et al., 1992) and variant-3 scorpion neurotoxin (Haydock et al., 1990). Finally and most interestingly, using the ten best conformers deduced by molecular modeling from ^{1}H NMR data, two sets of χ^1 angles were obtained either for Phe16 in the first finger or for Trp 37 in the second finger. In contrast, the χ^2 angles about the C^β-C^γ bond were more variable, suggesting that as in [Trp^2] oxytoxin the ground-state heterogeneity is probably correlated to χ^1 rotamers.

tRNA^{Phe}-binding properties of NCp7 13–30 F16W and NCp7 34–51

Using the fluorescence properties of Trp 16 and Trp 37 residues, we have monitored the binding of tRNA^{Phe} to the two zinc-saturated finger motifs of NCp7 and characterized the peptide-tRNA^{Phe} complexes. In both peptides, the binding of tRNA^{Phe} induced an almost complete quenching of Trp fluorescence. Fluorescence decay data and absorption difference spectra clearly suggest that this quenching corresponded to the stacking of the indole moiety of Trp with the bases of tRNA^{Phe}. This conclusion was corroborated by the −20 kJ/mol nonelectrostatic component of the binding energy measured in both peptides. This component is consistent with the theoretical estimates for the stacking energy of Trp with nucleotide bases (Kumar and Govil, 1984) and that of Phe 16 in NCp7 13–30-polyϵA interaction (Delahunty et al., 1992). From comparison of the sequences of the two fingers (Fig. 1) we infer that the aromatic amino acids are probably the major if not the sole residues involved in the nonelectrostatic interaction. Indeed, the other residues in both peptides are either not hydrophobic or not conserved. Thus, in contrast to polyϵA data (Delahunty et al., 1992), there is no direct evidence for the involvement of the amino acid immediately following the His zinc-binding residue since the hydrophobic Ile 24 residue of their peptide is replaced by nonhydrophobic Thr 24 and Asn 45 residues in our peptides. Moreover, as the same nonelectrostatic contribution was found for the interaction of the whole NCp7 with poly A (Khan and Giedroc, 1992), we speculate that the nonelectrostatic interaction of NCp7 with nucleotides is due primarily to the stacking of one or both aromatic residues with the bases. The intercalation of Trp within the bases also modifies the tRNA^{Phe} conformation, as can be observed from the strong negative band at 245 nm in the difference absorption spectra (Fig. 6). The amplitude of this band suggests that single-stranded regions of tRNA^{Phe} are essentially involved in the stacking interactions (Rajeswari et al., 1987).

At physiological concentrations of monovalent salt (about 0.1 M), the affinity of NCp7 13–30 F16W for tRNA^{Phe} (1×10^4 M^{-1}) was about threefold higher than the NCp7 34–51 affinity (Fig. 8 *b*). The nonelectrostatic interaction is clearly the main driving force for both peptides, and the higher affinity of the NH_2-terminal finger arises from additional electrostatic interactions (Table 2). Since about one ion pair is formed in the NCp7 13–30 F16W-tRNA^{Phe} interaction, we infer from sequence comparison (Fig. 1) that the residues involved in this mechanism are probably Lys 14 and/or Arg 29, since these two residues are replaced by noncharged Gly and Thr residues in NCp7 34–51. Interestingly, Lys 14 and Arg 29 were also inferred to interact with polyϵA (Delahunty et al., 1992) and were found to be crucial to cognate tRNA^{Lys,3} annealing to the initiation site of reverse transcription (De Rocquigny et al., 1992). The affinity of the NH_2-terminal finger for polyϵA at 0.1 M NaCl (Delahunty et al., 1992) is about one order of magnitude higher than that for tRNA^{Phe}. Moreover, the occluded binding site ($n = 1.75$) and the number of ion pairs formed ($m' = 2$) for polyϵA were also somewhat different. These discrepancies were tentatively interpreted to be arising from structural differences in nucleotides since tRNA^{Phe} was highly structured even in the absence of Mg^{2+} (Beardsley et al., 1970). In keeping with this hypothesis, the addition of 1 mM Mg^{2+}, which further increased the stability of tRNA^{Phe}, further reduced its affinity for the NH_2-terminal finger by decreasing the electrostatic interactions. Finally, in contrast to polyϵA, the structure of tRNA^{Phe} contains various single- and double-stranded regions. This implies that the binding sites are heterogeneous and may thus explain the noninteger number of ion pairs formed in certain circumstances (Table 2). Moreover, this heterogeneity may also explain the rather poor fits obtained in the presence of Mg^{2+}, since the equations of McGhee and von Hippel (1974) do not take into account the existence of sites with different affinities.

In conclusion, our experiments suggest that the aromatic amino acids in positions 16 and 37 are intrinsic tools well suited to monitoring the binding of nucleic acids and to characterizing the nucleotide-peptide complexes. Experiments are now in progress to determine whether the aromatic amino acids behave similarly in the NCp7 protein interaction with the heterologous tRNA^{Phe} and the homologous tRNA^{Lys,3}.

We are indebted to Prof H. Lami for his suggestions and help in lifetime measurements and to M. Wernert for her expert editorial assistance.
This work was supported by grants from the Agence Nationale de la Recherche sur le SIDA, Centre National de la Recherche Scientifique, and the Université Louis Pasteur.

REFERENCES

Alcala, J. R., E. Gratton, and F. G. Prendergast. 1987. Fluorescence lifetime distributions in proteins. *Biophys. J.* 51:597–604.

Aldovini, A., and R. A. Young. 1990. Mutations of RNA and protein sequences involved in HIV-1 packaging result in production of noninfectious virus. *J. Virol.* 64:1920–1926.

Barat, C., V. Lullien, O. Schatz, G. Keith, M. T. Nugeyre, F. Grüninger-Leitch, F. Barré-Sinoussi, S. F. J. Le Grice, and J. L. Darlix. 1989. HIV-1

reverse transcriptase specifically interacts with the anticodon domain of its cognate primer tRNA. *EMBO J.* 8:3279–3285.

Barat, C., S. F. J. Le Grice, and J. L. Darlix. 1991. Interaction of HIV-1 reverse transcriptase with a synthetic form of its replication primer, $tRNA^{Lys,3}$. *Nucleic Acids Res.* 19:751–757.

Beardsley, K., T. Tao, and C. R. Cantor. 1970. Studies on the conformation of the anticodon loop of phenylalanine transfer ribonucleic acid. Effect of environment on the fluorescence of the Y base. *Biochemistry.* 9:3524–3532.

Brooks, C. L., M. Karplus, and B. M. Pettitt. 1988. Proteins: a theoretical perspective of dynamics, structure and thermodynamics. *Adv. Chem. Phys.* 71:1–259.

Brun, F., J. J. Toulmé, and C. Hélène. 1975. Interactions of aromatic residues of proteins with nucleic acids. Fluorescence studies of the binding of oligopeptides containing tryptophan and tyrosine residues to polynucleotides. *Biochemistry.* 14:558–563.

Chabbert, M., W. Hillen, D. Hansen, M. Takahashi, and J. A. Bousquet. 1992. Structural analysis of the operator binding domain of Tn 10-encoded Tet repressor: a time-resolved fluorescence and anisotropy study. *Biochemistry.* 31:1951–1960.

Chang, M. C., J. W. Petrich, D. B. Mc Donald, and G. R. Fleming. 1983. Nonexponential fluorescence decay of tryptophan, tryptophylglycine, and glycyltryptophan. *J. Am. Chem. Soc.* 105:3819–3824.

Chen, R. F., J. R. Knutson, H. Ziffer, and D. Porter. 1991. Fluorescence of tryptophan dipeptides: correlations with the rotamer model. *Biochemistry.* 30:5184–5195.

Cockle, S. A., and A. G. Szabo. 1981. Time-resolved fluorescence spectra of tryptophan in monomeric glucagon. *Photochem. Photobiol.* 34:23–27.

Darlix, J. L., C. Gabus, M. T. Nugeyre, F. Clavel, and F. Barré-Sinoussi. 1990. *Cis* elements and *trans*-acting factors involved in the RNA dimerization of the human immunodeficiency virus HIV-1. *J. Mol. Biol.* 216: 689–699.

De Rocquigny, H., D. Ficheux, C. Gabus, M. C. Fournié-Zaluski, J. L. Darlix, and B. P. Roques. 1991. First large scale chemical synthesis of the 72 amino acids HIV-1 nucleocapsid protein NCp7 in an active form. *Biochem. Biophys. Res. Commun.* 180:1010–1018.

De Rocquigny, H., C. Gabus, A. Vincent, M. C. Fournié-Zaluski, B. P. Roques, and J. L. Darlix. 1992. Viral RNA annealing activities of HIV-1 nucleocapsid protein require only peptide domains outside the zinc fingers. *Proc. Natl. Acad. Sci. USA.* 89:6472–6476.

Delahunty, M. D., T. L. South, M. F. Summers, and R. L. Karpel. 1992. Nucleic acid interactive properties of a peptide corresponding to the N-terminal zinc finger domain of HIV-1 nucleocapsid protein. *Biochemistry.* 31:6461–6469.

Di Marzo Veronese, F., R. Rahman, T. D. Copeland, S. Oroszlan, R. C. Gallo, and M. G. Sarngadharan. 1987. Immunological and chemical analysis of P6, the carboxyl-terminal fragments of HIVP15. *AIDS Res. Hum. Retroviruses.* 3:253–264.

Dupraz, P., S. Oertle, C. Méric, P. Damay, and P. F. Spahr. 1990. Point mutations in the proximal Cys-His box of Rous sarcoma virus nucleocapsid protein. *J. Virol.* 64:4978–4987.

Eftink, M. R., and C. A. Ghiron. 1976. Exposure of tryptophanyl residues in proteins. Quantitative determination by fluorescence quenching studies. *Biochemistry.* 15:672–680.

Eisinger, J., and G. Navon. 1969. Fluorescence quenching and isotope effect of tryptophan. *J. Chem. Phys.* 50:2069–2077.

Fitzgerald, D. W., and J. E. Coleman. 1991. Physicochemical properties of cloned nucleocapsid protein from HIV. Interactions with metal ions. *Biochemistry.* 30:5195–5201.

Frauenfelder, H., F. Parak, and R. D. Young. 1988. Conformational substates in proteins. *Annu. Rev. Biophys. Chem.* 17:451–479.

Green, S. M., J. R. Knutson, and P. Hensley. 1990. Steady-state fluorescence and time-resolved fluorescence monitor changes in tryptophan environment in arginase from *Saccharomyces cerevisiae* upon removal of catalytic and structure metal ions. *Biochemistry.* 29:9159–9168.

Haydock, C., J. C. Sharp, and F. G. Prendergast. 1990. Tryptophan-47 rotational isomerization in variant-3 scorpion neurotoxin. A combination thermodynamic perturbation and umbrella sampling study. *Biophys. J.* 57:1269–1279.

Hélène, C., F. Brun, and M. Yaniv. 1971. Fluorescence studies of interactions between *Escherichia coli* valyl-tRNA synthetase and its substrates. *J. Mol. Biol.* 58:349–365.

Hopfield, J. J. 1974. Electron tranfer between biological molecules by thermally activated tunneling. *Proc. Natl. Acad. Sci. USA.* 71:3640–3644.

Hopfield, J. J. 1977. Photo-induced charge transfer. A critical test of the mechanism and range of biological electron transfer processes. *Biophys. J.* 18:311–321.

Khan, R., and D. P. Giedroc. 1992. Recombinant human immunodeficiency virus type 1 nucleocapsid (NC^{p7}) protein unwinds tRNA. *J. Biol. Chem.* 267:6689–6695.

Kolber, Z. S., and M. D. Barkley. 1986. Comparison of approaches to the instrumental response function in fluorescence decay measurements. *Anal. Biochem.* 152:6–21.

Kowalczykowski, S. C., L. S. Paul, N. Lonberg, J. W. Newport, J. A. McSwiggen, and P. H. von Hippel. 1986. Cooperative and noncooperative binding of protein ligands to nucleic acid lattices: experimental approaches to the determination of thermodynamic parameters. *Biochemistry.* 25:1226–1240.

Kumar, N. V., and G. Govil. 1984. Theoretical studies on protein-nucleic acid interactions. III. Stacking of aromatic amino acids with bases and base pairs of nucleic acids. *Biopolymers.* 23:2009–2024.

Lakowicz, J. R. 1983. Principles of Fluorescence Spectroscopy. Plenum Press, New York. 383–431.

Lami, H., and E. Piémont. 1992. Fluorescence decay analysis by iterative reconvolution based on the estimated covariance matrix. *Chem. Phys.* 163:149–159.

McGhee, J. D., and P. H. von Hippel. 1974. Theoretical aspects of DNA-protein interactions: co-operative and non-co-operative binding of large ligands to a one-dimensional homogeneous lattice. *J. Mol. Biol.* 86:469–489.

Mély, Y., H. de Rocquigny, E. Piémont, H. Déméné, N. Jullian, M. C. Fournié-Zaluski, B. Roques, and D. Gérard. 1993. Influence of the N- and C-terminal chains on the zinc-binding and conformational properties of the central zinc-finger structure of Moloney murine leukaemia virus nucleocapsid protein: a steady-state and time-resolved fluorescence study. *Biochim. Biophys. Acta.* 1161:6–18.

Méric, C., and S. P. Goff. 1989. Characterization of Moloney murine leukaemia virus mutants with single-amino-acid substitutions in the Cys-His box of the nucleocapsid protein. *J. Virol.* 63:1558–1568.

Montenay-Garestier, T., F. Toulmé, J. Fidy, J. J. Toulmé, T. Le Doan, and C. Hélène. 1983. Structure and dynamics of peptide-nucleic acid complexes. *In* Structure, Dynamics, Interactions and Evolution of Biological Macromolecules. C. Hélène, editor. D. Reidel Publishing Company, Dordrecht, the Netherlands. 113–128.

Morellet, N., N. Jullian, H. De Rocquigny, B. Maigret, J. L. Darlix, and B. P. Roques. 1992. Determination of the structure of the nucleocapsid protein NCp7 from human immunodeficiency virus type 1 by ^1H NMR. *EMBO J.* 11:3059–3065.

Omichinski, J. G., G. M. Clore, K. Sakaguchi, E. Appella, and A. M. Gronenborn. 1991. Structural characterization of a 39-residue synthetic peptide containing the two zinc binding domains from the HIV-1 p7 nucleocapsid protein by CD and NMR spectroscopy. *FEBS Lett.* 292:25–30.

Petrich, J. W., M. C. Chang, D. B. McDonald, and G. R. Fleming. 1983. On the origin of nonexponential fluorescence decay in tryptophan and its derivatives. *J. Am. Chem. Soc.* 105:3824–3832.

Rajeswari, M. R., T. Montenay-Garestier, and C. Hélène. 1987. Does tryptophan intercalate in DNA? A comparative study of peptide binding to alternating and nonalternating A·T sequences. *Biochemistry.* 26:6825–6831.

Record, M. T., T. M. Lohman, and P. de Haseth. 1976. Ion effects on ligand-nucleic acid interactions. *J. Mol. Biol.* 107:145–158.

Ricci, R. W. 1970. Deuterium-isotope effect on the fluorescence yields and lifetimes of indole derivatives—including tryptophan and tryptamine. *Photochem. Photobiol.* 12:67–75.

Robbins, R. J., G. R. Fleming, G. S. Beddard, G. W. Robinson, P. J. Thistlethwaite, and G. J. Woolfe. 1980. Photophysics of aqueous tryptophan: pH and temperature effects. *J. Am. Chem. Soc.* 102:6271–6279.

Ross, J. B. A., K. W. Rousslang, and L. Brand. 1981. Time-resolved fluorescence and anisotropy decay of the tryptophan in adrenocorticotropin-(1–24). *Biochemistry.* 20:4361–4369.

Ross, J. B. A., H. R. Wyssbrod, R. A. Porter, G. P. Schwartz, C. A. Michaels, and W. R. Laws. 1992. Correlation of tryptophan fluorescence intensity decay parameters with ^{1}H-NMR-determined rotamer conformations: [tryptophan^2] oxytocin. *Biochemistry.* 31:1585–1594.

South, T. L., P. R. Blake, R. C. Sowder, L. O. Arthur, L. E. Henderson, and M. F. Summers. 1990. The nucleocapsid protein isolated from HIV-1 particles binds zinc and forms retroviral-type zinc fingers. *Biochemistry.* 29:7786–7789.

South, T. L., P. R. Blake, D. R. Hare, and M. F. Summers. 1991. C-terminal retroviral-type zinc finger domain from the HIV-1 nucleocapsid protein is structurally similar to the N-terminal zinc finger domain. *Biochemistry.* 30:6342–6349.

Summers, M. F., T. L. South, B. Kim, and D. R. Hare. 1990. High-resolution structure of an HIV zinc fingerlike domain via a new NMR-based distance geometry approach. *Biochemistry.* 29:329–340.

Summers, M. F., L. E. Henderson, M. R. Chance, J. W. Bess, Jr., T. L. South, P. R. Blake, I. Sagi, G. Perez-Alvarado, R. C. Sowder, D. R. Hare, and L. O. Arthur. 1992. Nucleocapsid zinc fingers detected in retroviruses: EXAFS studies of intact viruses and the solution-state structure of the nucleocapsid protein from HIV-1. *Protein Sci.* 1:563–574.

Szabo, A. G., and D. M. Rayner. 1980. Fluorescence decay of tryptophan conformers in aqueous solution. *J. Am. Chem. Soc.* 102:554–563.

Toulmé, F., and C. Hélène. 1980. Complexes d'empilement du tryptophane avec les bases nucléiques: absorption induite. *J. Chim. Phys.* 9:855–859.

Werner, T. C., and L. S. Forster. 1979. The fluorescence of tryptophyl peptides. *Photochem. Photobiol.* 29:905–914.